Accepted to AJ: September 26, 2014
Preprint typeset using LaTeX style emulateapj v. 5/2/11

A DEEP PROPER MOTION CATALOG WITHIN THE SLOAN DIGITAL SKY SURVEY FOOTPRINT

Jeffrey A. Munn and Hugh C. Harris
US Naval Observatory, Flagstaff Station, 10391 W. Naval Observatory Road, Flagstaff, AZ 86005-8521; jam@nofs.navy.mil, hch@nofs.navy.mil

Ted von Hippel
Embry-Riddle Aeronautical University, Physical Sciences, 600 S. Clyde Morris Blvd, Daytona Beach, FL 32114-3900; ted.vonhippel@erau.edu

Mukremin Kilic
University of Oklahoma, Homer L. Dodge Department of Physics and Astronomy, 440 W. Brooks Street, Norman, OK 73019; kilic@ou.edu

James W. Liebert
University of Arizona, Steward Observatory, Tucson, AZ 85721; jamesliebert@gmail.com

Kurtis A. Williams
Department of Physics and Astronomy, Texas A&M University–Commerce, P.O. Box 3011, Commerce, TX 75429; kurtis.williams@tamuc.edu

Steven DeGenarro
Department of Astronomy, University of Texas at Austin, 1 University Station C1400, Austin, TX 78712-0259; studiofortytwo@yahoo.com

Elizabeth Jeffery
BYU Department of Physics and Astronomy, N283 ESC, Provo, UT 84602; ejeffery@byu.edu

and

Trudy M. Tilleman
US Naval Observatory, Flagstaff Station, 10391 W. Naval Observatory Road, Flagstaff, AZ 86005-8521; trudy@nofs.navy.mil
Accepted to AJ: *September 26, 2014*

ABSTRACT

A new proper motion catalog is presented, combining the Sloan Digital Sky Survey (SDSS) with second epoch observations in the r band within a portion of the SDSS imaging footprint. The new observations were obtained with the 90prime camera on the Steward Observatory Bok 90 inch telescope, and the Array Camera on the U.S. Naval Observatory, Flagstaff Station, 1.3 meter telescope. The catalog covers 1098 square degrees to $r = 22.0$, an additional 1521 square degrees to $r = 20.9$, plus a further 488 square degrees of lesser quality data. Statistical errors in the proper motions range from 5 mas year^{-1} at the bright end to 15 mas year^{-1} at the faint end, for a typical epoch difference of 6 years. Systematic errors are estimated to be roughly 1 mas year^{-1} for the Array Camera data, and as much as 2 – 4 mas year^{-1} for the 90prime data (though typically less). The catalog also includes a second epoch of r band photometry.

Subject headings: astrometry — catalogs — proper motions — surveys

1. INTRODUCTION

Wide area, deep proper motion catalogs have wide applicability to studies of the structure and formation of our Galaxy. Most current catalogs are based on photographic surveys done with the various 1 meter-class Schmidt telescopes, including the Palomar Oschin 1.2 meter (POSS-I and POSS-II), the European Southern Observatory 1.0 meter (ESO surveys), and the United Kingdom 1.2 meter Schmidt Telescope (SERC and AAO surveys). Recent proper motion catalogs based on these Schmidt plates include USNO-B (Monet et al. 2003) and the LSPM high proper motion catalog (Lépine & Shara 2005). These catalogs are limited by the depth of the Schmidt plates to $V \sim 20$.

The Sloan Digital Sky Survey (SDSS; York et al. 2000; Gunn et al. 1998, 2006; Fukugita et al. 1996) is the modern successor to the Schmidt surveys. Using CCDs rather than photographic plates, SDSS provides 5-band ($ugriz$) imaging over 14,555 square degrees, with a 95% completeness rate for point sources of $r = 22.2$, thus reaching roughly 2 magnitudes fainter than the Schmidt surveys. However, SDSS is primarily a single epoch survey, and thus proper motions cannot be derived from SDSS data alone. While a number of studies have combined

SDSS with USNO-B to produce improved proper motions (e.g., Munn et al. 2004; Gould & Kollmeier 2004), these are still limited to the depth of the Schmidt plates.

This paper presents new observations targeting 3100 square degrees in the SDSS footprint, separated in epoch from the SDSS observations by typically 5 – 10 years. These are combined with SDSS astrometry to create a new proper motion catalog, extending 1 – 2 magnitudes fainter than the Schmidt based catalogs. The immediate science driver for the new catalog is to extend the work of Harris et al. (2006) on the white dwarf luminosity function, with the goal of greatly increasing samples of the coolest disk white dwarfs as well as thick disk and halo white dwarfs (see Kilic et al. 2010 for three halo white dwarfs discovered in this survey). Moreover, the catalog should be broadly useful for a range of Galactic and stellar research.

2. OBSERVATIONS

The initial survey was conducted using the 90prime prime focus wide-field imager on the Steward Observatory Bok 90 inch telescope (Williams et al. 2004). 90prime is a mosaic of four Lockheed 4k by 4k CCDs, with a $1.16^\circ \times 1.16^\circ$ edge-to-edge field-of-view (FOV), an imaging area of 1.06 square degrees, inter-CCD gaps in both dimensions of 0.131°, and a plate scale of 0.45 arcsec per pixel. 2107 observations were obtained over 45 nights from 2006 to 2008. Each target field was observed once in the SDSS r filter (except for the night UT 2006 January 2, when the Bessell R filter was accidentally used). Exposure times were 5 minutes in good conditions, and up to 15 minutes in cloudy weather or bad seeing. Field centers were separated by one degree in both right ascension and declination.

There were a number of complications with the 90prime instrument at the time of the observations, all of which have since been largely corrected. The focal plane was populated with experimental CCDs, which have since been replaced. There was a large charge trap on CCD 3, rendering data in the region $1560 < x < 2700$ and $y > 2530$ unusable. One amp on CCD 2, covering half of the chip ($x > 2048$), displays a pattern noise, evident as low level striping parallel to the x (declination) axis. While the astrometry and photometry are usually only minimally affected, for the nights of 2007 May 25 – 26 and June 11 – 12, the pattern noise was bad enough that data on that half of the chip was unusable. There were some pointing issues, causing some observations to not completely cover the intended target field. Finally, the Bok telescope required refocusing and recollimation any time the telescope was slewed through large angles. Evidence for instability in the focus and/or collimation, and its effects on the astrometry, will be discussed below.

Starting in 2009, observations were obtained using the Array Camera on the U.S. Naval Observatory, Flagstaff Station, 1.3 meter telescope. The Array Camera is a 2 x 3 mosaic of 2048 x 4102 e2v CCDs with $0.6''$ pixels, and a field of view of 1.41° in right ascension (with inter-CCD gaps of 0.062°) by 1.05° in declination (with inter-CCD gaps of 0.019°). 2532 observations were obtained over 179 nights from 2009 – 2011, using 20 minute exposure times. Field centers were separated by 1.4 degrees in right ascension and 1.0 degrees in declination. As with the Bok, there were some pointing issues with the 1.3m at the time which caused some observations to not completely cover their intended target field.

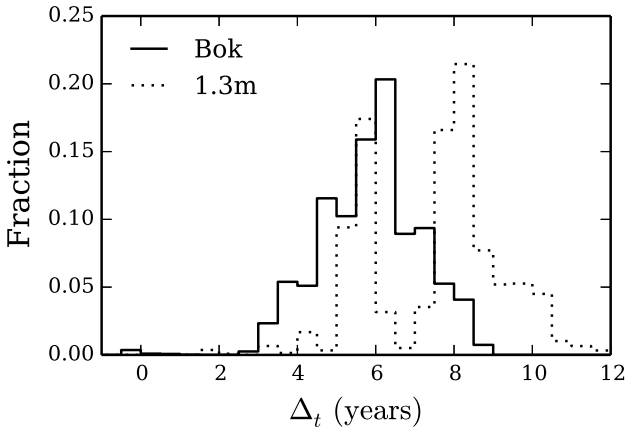

Figure 1. Distribution of epoch differences between the SDSS observations and this survey's observations, for representative samples of stars in the Bok (solid histogram) and 1.3m (dotted histogram) surveys.

Target fields were chosen so as to maximize the epoch difference between the SDSS observations and this survey's observations, and thus minimize the proper motion errors. Each survey field is covered by more than one SDSS scan, and thus stars within a given field will have different epoch differences. Figure 1 plots the distribution of epoch differences for a representative sample of stars, separately for the Bok and 1.3m surveys. 75% of the Bok survey, and 97% of the 1.3m survey, have epoch differences greater than 5 years.

3. DATA PROCESSING

Each observation generates four (for 90prime) or six (for Array Camera) images, one image for each CCD in the camera. Each image is processed separately, throughout all steps in the data processing.

3.1. *Object Detection and Characterization*

Images were bias subtracted and flat-field corrected using the Image Reduction and Analysis Facility (IRAF; Tody 1986, 1993)[1]. Median object flats were used to flat-field correct the Bok images, while median twilight flats were used for the 1.3m images. SExtractor (Bertin & Arnouts 1996) was then used to detect and characterize the objects in the images. Object detection used a detection threshold of 1.5 times the background rms, after convolution with a Gaussian with a FWHM of 3 pixels. Object detection was also performed using DAOPHOT II (Stetson 1987), which does a better job detecting stars near overexposed stars. The merged SExtractor and DAOPHOT detections were then fed to DAOPHOT, which was used to model the point-spread function (PSF), and to measure PSF magnitudes based on that model PSF. The PSF was allowed to vary quadratically across each image.

3.2. *Astrometric Calibration*

[1] IRAF is distributed by the National Optical Astronomy Observatories, which are operated by the Association of Universities for Research in Astronomy, Inc., under cooperative agreement with the National Science Foundation.

The SDSS Seventh Data Release (DR7; Abazajian et al. 2009) was used to provide calibration stars to both astrometrically and photometrically calibrate the observations, as well as to provide the first epoch positions for the proper motions. At the time of this work, both SDSS DR8 (Aihara et al. 2011) and DR9 (Ahn et al. 2012) were also available. DR8 introduced some bugs in the astrometric processing, leading to less accurate astrometry for some objects (this has been corrected in subsequent data releases). DR9 uses a different algorithm from prior releases to choose the primary detection of an object which has been observed more than once. The new algorithm has the effect that, in some regions of sky, DR9 uses more recent observations than those used in DR7, leading to a shorter epoch difference between the SDSS primary observation and our observation, and thus less accurate derived proper motions. DR7 represents the best choice to maximize both the quality of the astrometry and the epoch difference with our observations.

For use as calibration stars, the SDSS positions must be propagated to the epoch of our observations. This is done using the proper motions from the SDSS+USNO-B catalog (Munn et al. 2004, 2008), which recalibrates the individual plate detections in USNO-B using SDSS galaxies, and then combines those recalibrated positions with the SDSS positions to derive improved proper motions. The random errors for the SDSS+USNO-B proper motions vary from about 2.8 – 4.7 mas year^{-1} over the magnitude range $17 < r < 20$ from which calibration stars are selected, while the systematic errors are typically of order 0.2 mas year^{-1}, though they can be 2 – 3 times larger in some patches of sky (Bond et al. 2010).

The astrometric calibrations use the DAOPHOT centers measured by fitting the PSF to each star. An astrometrically clean set of calibration stars is selected, by requiring that (1) they pass the set of criteria suggested on the SDSS DR7 Web site for defining a clean sample of point sources[2]; (2) their r magnitude be in the range 17 – 20, so as to avoid saturated stars and stars with large centering errors; (3) their $r-i$ color be in the range -0.5 – 2, for which differential chromatic refraction (DCR) can be well-modelled as a linear function of $r-i$; and (4) their SDSS+USNO-B proper motions be well measured, following the prescription given in Kilic et al. (2006). There are a minimum of 100 calibrating stars per image, and more typically 200 – 400. The tangent plane coordinates of the calibration stars, ξ and η, are fit as functions of image coordinate x and y, using the following formulae:

$$x' = x + (c_0 + c_1 \tan z \cos q)(r-i) + m_0(x,y), \quad (1)$$

$$y' = y + (c_0 + c_1 \tan z \sin q)(r-i) + m_1(x,y), \quad (2)$$

$$\xi = a_0 + a_1 x' + a_2 y' + a_3 x'^2 + a_4 x' y' + a_5 y'^2 + a_6 x'^3 + a_7 x' y'^2 + a_8 x'^2 y' + a_9 y'^3, \quad (3)$$

$$\eta = b_0 + b_1 x' + b_2 y' + b_3 x'^2 + b_4 x' y' + b_5 y'^2 + b_6 x'^3 + b_7 x' y'^2 + b_8 x'^2 y' + b_9 y'^3. \quad (4)$$

Equations (1) and (2) correct the raw image coordinates for effects which are stable across many runs, including DCR and high order optical distortions. In equations (1) and (2), x and y are the image coordinates of the star, x' and y' are the corrected coordinates, z is the zenith distance, q is the parallactic angle, r and i are the SDSS magnitudes, c_i are the corrections for DCR, and m_i are residual maps used to correct high order optical distortions. These corrected image coordinates are then fit to the calibration star tangent plane coordinates ξ and η in equations (3) and (4), using cubic polynomials.

[2] See http://www.sdss.org/dr7/products/catalogs/flags.html

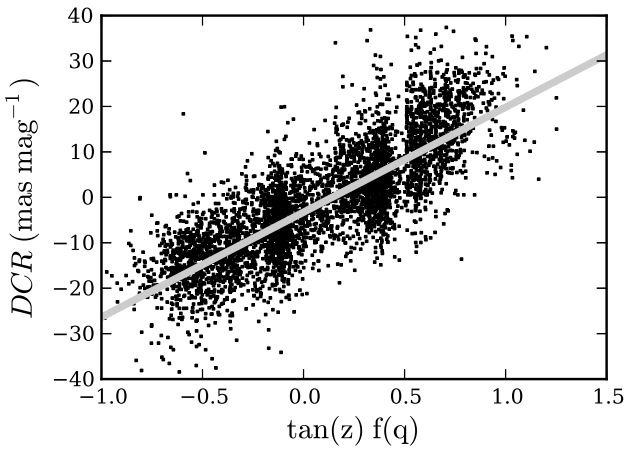

Figure 2. Differential chromatic refraction (DCR), measured along both the x and y axes, for all images in the 1.3m survey, plotted against a factor proportional to the expected total refraction along that axis (the total refraction is proportional to the tangent of the zenith distance, z, and $f(q)$ accounts for the component of DCR along each axis, where q is the parallactic angle, and $f(q)$ is cos(q) for the the x-axis and sin(q) for the y-axis).

To derive the correction terms c_i and m_i in equations (1) and (2), equations (3) and (4) are first solved for each image, using uncorrected image coordinates. For each image, DCR is then solved for by fitting the residuals in x and y, separately, as linear functions of $r-i$. Since this is a noisy measurement for individual frames, we then fit the ensemble of the measured DCR for all images (separately for each survey) against the expected total atmospheric refraction along the axis (which is proportional to the tangent of the zenith distance, with the component along each axis determined by the parallactic angle). The results for the 1.3m are shown in Figure 2 (the results for the Bok are similar). This fit determines the values of c_o and c_1 in equations (1) and (2). DCR corrections are fairly small in the SDSS r filter, amounting to less than 20 mas mag^{-1} for both surveys at a zenith distance of 45 degrees. There is measurable DCR even at the zenith, where no atmospheric DCR is to be expected, of 4.4 mas mag^{-1} for the 90prime and 3.3 mas mag^{-1} for the 1.3m; this is not currently understood, but we note that both cameras feature refractive field correctors.

After applying the DCR corrections, residual maps were created by measuring the mean residuals across multiple nights, binned across the focal plane. For the 1.3m, a single residual map was used for the entire survey, except for one dark run comprising nine nights of observations from 2009 April 19 through May 1, for which there were clear remaining systematic residuals on CCD 4, and thus a different residual map was used for that CCD only. We suspect there was a problem with the primary mirror support system during that run. For the Bok, separate residual maps were used for the 2006 and

2007 runs, and the 2008 runs. Figures 3 and 4 display the residual maps for the Bok (2008 runs) and 1.3m, respectively. These residual maps are then used to correct the raw image coordinates for high order optical distortions (the m_i terms in equations (1) and (2)).

Finally, the plate solutions for the individual images (equations (3) and (4)) are rederived, now using coordinates corrected for DCR and high order optical distortions (equations (1) and (2)). Proper motions are then calculated by simply differencing our positions and the positions of the matching SDSS DR7 primary detections.

The stability of the high order optical distortions was monitored by examining residual maps averaged over individual observing runs and, for the Bok survey, individual nights (due to the longer exposure times for the 1.3m, there aren't enough observations in individual nights to generate statistically significant residual maps). For the Bok survey, variable large scale systematic errors across the focal plane are seen, of up to 10 — 20 mas (though typically considerably less over most of the FOV), both from observing run to observing run, as well as night to night within observing runs. The greatest variability is seen for the declination residuals on CCDs 2 and 4. While much of the data are better than this, these variable residuals represent a source of irreducible field-dependent systematic error. These can introduce systematic errors in the proper motions of up to 4 mas year^{-1} (though more typically half that), dependent on position in the focal plane, and varying in time. There are not enough calibration stars on individual exposures to remove these time-dependent variations in the residual maps. The 1.3m shows no such run-to-run variations, with the exception of the single dark run discussed above. However, again due to the considerably smaller number of exposures taken per night on the 1.3m, it is not possible to look for night-to-night variations.

The errors in the calibrations may be characterized by the rms residuals in the final fits for each image, limited to bright unsaturated stars ($17 < r < 18$ for the Bok survey, $16.5 < r < 18$ for the 1.3m survey) for which centering errors make negligble contributions. Figure 5 displays histograms of the rms residuals for each image, separately for each survey, and separately in right ascension and declination. The distributions peak at 30 and 35 mas for the Bok and 1.3m surveys, respectively.

3.3. *Photometric Calibration*

DAOPHOT PSF magnitudes were calibrated directly against SDSS PSF magnitudes, using sets of SDSS calibration stars similar to those used for the astrometric calibrations, over the magnitude range $17 < r < 20$. The PSF varies considerably over the large FOVs of both telescopes, thus the calibration is dependent on the stars' positions in the FOV. The PSF magnitudes were first corrected for color terms, using a separate correction for each survey, linear with $r-i$, and constant over each survey. For each image separately, a two-dimensional cubic surface was fit to the differences between the SDSS PSF magnitudes and color-corrected DAOPHOT magnitudes, using the formula

$$r_{sdss} - r'_{psf} = a_0 + a_1 x + a_2 y + a_3 x^2 + a_4 xy + a_5 y^2 + a_6 x^3 + a_7 xy^2 + a_8 x^2 y + a_9 y^3, \quad (5)$$

where r_{sdss} is the SDSS PSF magnitude, r'_{psf} is the color-corrected DAOPHOT PSF magnitude, and x and y are the image coordinates of the star. There are a minimum of 200 calibrating stars per image, and more typically 400 – 600.

The calibration errors may be estimated using the rms residuals for the brighter calibration stars ($r < 18$). Figure 6 displays histograms for the estimated calibration errors. Separate histograms are displayed for "good" and "ok" fields (defined below). The calibrations are better for the 1.3m, with the distribution peaking around 0.018 mag.

4. RESULTS

4.1. *Survey Coverage and Depth*

Individual exposures were assigned one of three quality ratings. "Good" fields were taken under photometric conditions, in reasonable seeing (less than 2.5 arcsec for the Bok survey, less than 3 arcsec for the 1.3m survey), have acceptable pointing errors, have astrometric calibration errors of less than 60 mas in both right ascension and declination, and have a minimum of 0.09 square degrees of SDSS coverage. "Ok" fields have the same requirements on the astrometric calibration errors and SDSS coverage, but can have up to half a magnitude of extinction due to clouds, seeing up to 4 arcsecs, and have no restrictions on pointing errors. The remaining observations are declared "bad", and are not included in the catalog. For the Bok, 78.3% of the observations were "good", 14.7% were "ok", and 7.0% were "bad". For the 1.3m, 67.7% of the observations were "good", 15.4% were "ok", and 16.9% were "bad".

The r magnitude at which a given field reaches 90% completeness is well approximated for the Bok by the formula

$$r_{90} = 22.33 - 0.5(\text{seeing} - 1.5) + 0.5(\text{sky} - 21.03) + (\text{zeropt} - 6.40), \quad (6)$$

and for the 1.3m by the formula

$$r_{90} = 21.61 - 0.5(\text{seeing} - 2.0) + 0.5(\text{sky} - 20.48) + (\text{zeropt} - 4.57), \quad (7)$$

where "seeing" is the seeing in arcsecs, "sky" is the sky brightness in mag arcsec^{-2}, and "zeropt" is the photometric zero point, which serves as a measure of the extinction due to clouds. The Bok benefits from both better seeing than the 1.3m (typical seeing of 1.5 arcsec versus 2.0 arcsec) and darker skies (typical sky brightness of 21.0 mag arcsec^{-2} versus 20.5 mag arcsec^{-2}), leading to the Bok reaching about a magnitude fainter than the 1.3m. Figure 7 displays the mean completeness versus magnitude for the "good" fields in both surveys. The Bok survey is 90% complete to 22.3, and 95% complete to 22.0. The 1.3m survey is 90% complete to 21.3, and 95% complete to 20.9. The incompleteness at the bright end reflects the onset of saturation at $r = 16$ for the Bok and $r = 15$ for the 1.3m.

Some target fields have more than one observation. In those cases, the observation with the deepest estimated completeness is included in the survey. The set of "good" fields, of fairly uniform depth, comprises the primary product of this survey, with the set of "ok" fields comprising a secondary product of varying and lesser depth. The

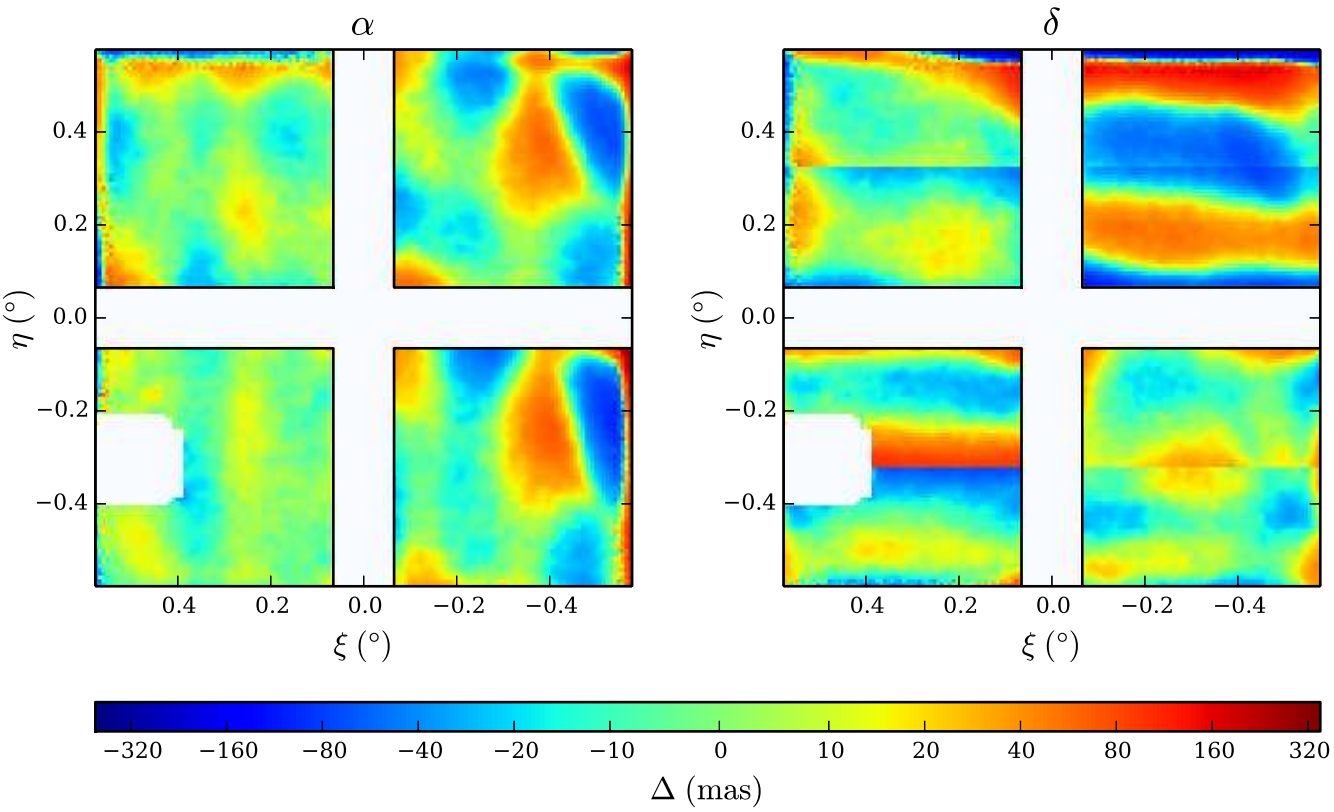

Figure 3. Map showing the mean residuals (catalog - observed, in mas) across the focal plane for the 2008 Bok runs. Residuals in right ascension are shown in the left figure, and in declination in the right figure.

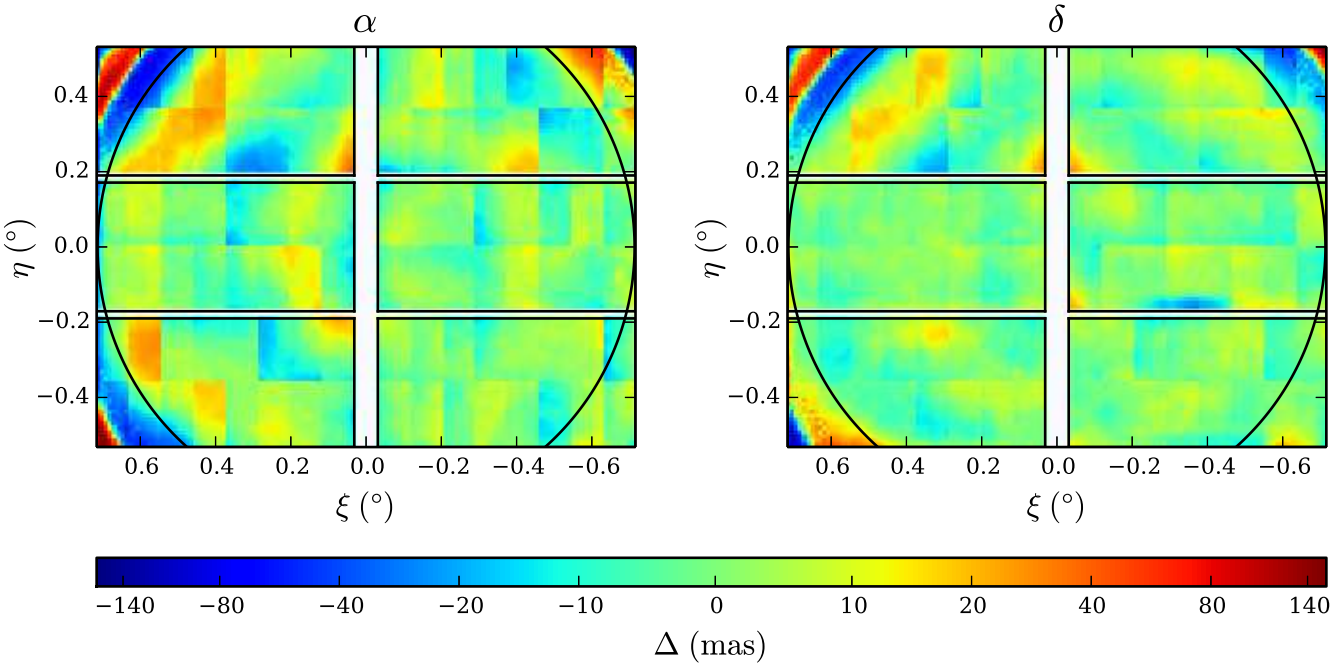

Figure 4. Map showing the mean residuals (catalog - observed, in mas) across the focal plane for the 1.3m survey. Residuals in right ascension are shown in the left figure, and in declination in the right figure. A circle with radius 0.7 degrees is shown for reference.

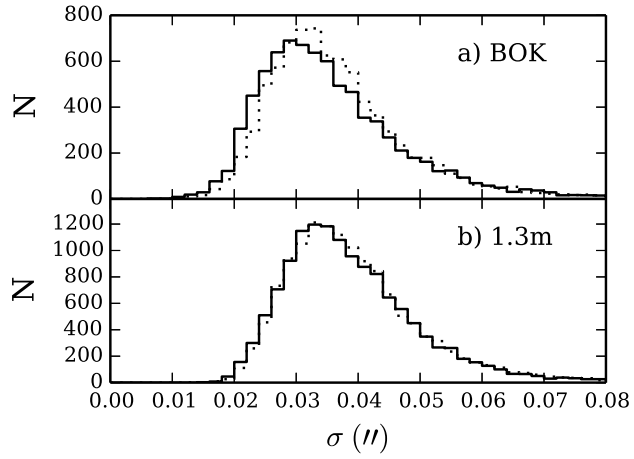

Figure 5. Distribution of astrometric calibration errors for each image, for the Bok (panel (a)) and 1.3m (panel (b)) surveys. The distributions in right ascension (solid histograms) and declination (dotted histograms) are displayed separately.

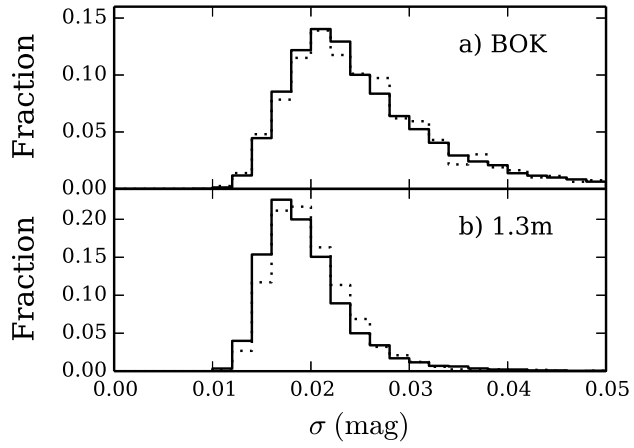

Figure 6. Distribution of photometric calibration errors for each image, for the Bok (panel (a)) and 1.3m (panel (b)) surveys. Solid and dotted histograms are the distributions for "good" and "ok" fields, respectively.

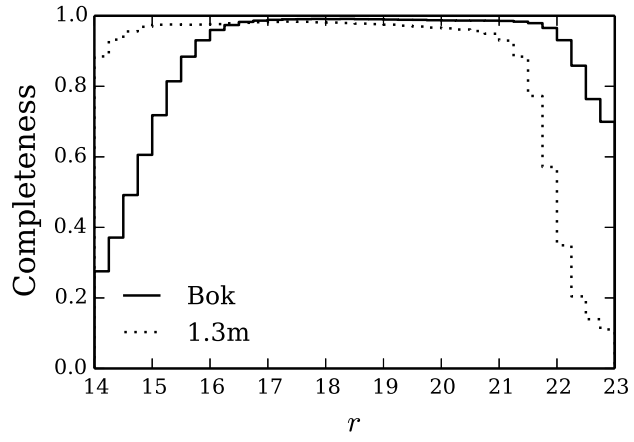

Figure 7. Completeness in the "good" fields for the Bok (solid histogram) and 1.3m (dotted histogram) surveys.

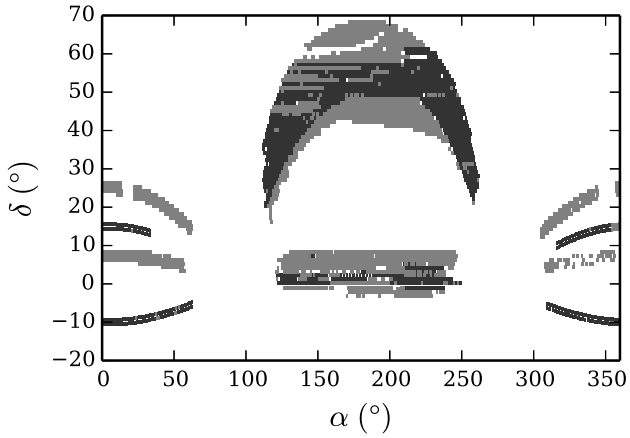

Figure 8. Sky coverage of the survey, including both "good" and "ok" observations. Dark and light regions indicate Bok and 1.3m coverage, respectively.

"good" fields from the Bok survey cover 1097.9 square degrees of sky, while the "ok" fields add another 145.6 square degrees. The "good" fields from the 1.3m survey cover 1521.4 square degrees of sky, while the "ok" fields add another 342.6 square degrees. The sky coverage is displayed in Figure 8.

4.2. *Proper Motions*

QSOs are morphologically stellar, yet distant enough to have undetectable proper motions to the accuracy of this survey. The distribution of measured proper motions for a sample of QSOs thus provides a simple test of the accuracy of the measured proper motions. All analysis in this section uses the SDSS Data Release 7 catalog of spectroscopically confirmed QSOs (Schneider et al. 2010). The QSO sample is limited to those with clean detections in both SDSS and this survey, by requiring that (1) the SDSS detection meets the criteria for a "clean" point source as recommended on the SDSS DR7 website; (2) it has a clean detection in this survey as indicated by the SExtractor flags; (3) its observation in this survey has a quality of "good"; and (4) it has an epoch difference of at least 4 years. This yields a sample of 10855 QSOs in the Bok survey footprint, and 12621 in the 1.3m survey footprint.

The accuracy of the proper motion error estimates is first examined by binning the QSOs in half magnitude bins in the range $17.5 < r < 21$, and within each bin examining the distribution of the proper motions, divided by the errors in the proper motions, separately in right ascension and declination. If the error estimates are accurate the distribution in each bin should be a Gaussian with a standard deviation of one. The distribution in each bin is well represented by a Gaussian. Figure 9 plots the standard deviation of the fitted Gaussian in each bin against r magnitude. The errors are overestimated by 10 — 15% at bright magnitudes, becoming more accurate towards fainter magnitudes. The calibration errors are thus likely somewhat overestimated, as they dominate the errors at bright magnitudes (the centering errors become comparable to the calibration errors around $r \sim 21$).

The dependence of proper motion errors on magnitude is shown in Figure 10. The mean proper motion errors

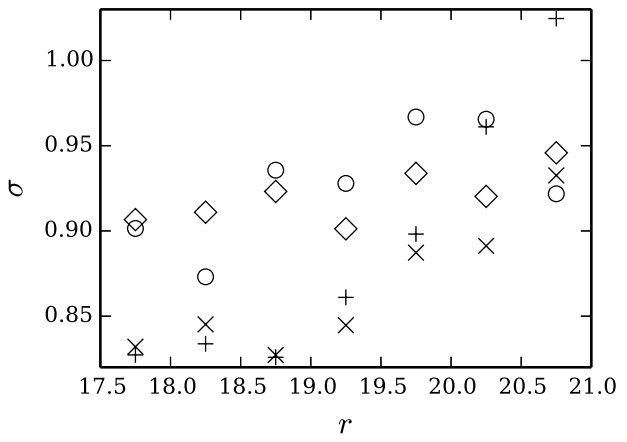

Figure 9. Standard deviation of the distribution of QSO proper motions divided by proper motion errors, in half-magnitude bins. Circles and diamonds are the standard deviations in right ascension and declination, respectively, for the Bok survey. Pluses and crosses are the standard deviations in right ascension and declination, respectively, for the 1.3m survey. Perfectly estimated errors would yield a standard deviation of one.

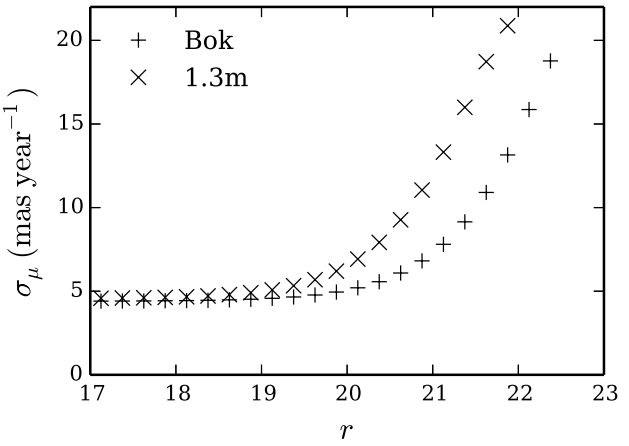

Figure 10. Mean proper motion error (averaged over the right ascension and declination components), scaled to an epoch difference of 6 years, as a function of r magnitude, for a sample of clean stars with a field quality of "good". Pluses and crosses are for the Bok and 1.3m surveys, respectively.

(averaged over the right ascension and declination components) for a sample of clean stars in fields of quality "good", scaled to a typical epoch difference of 6 years, are plotted in quarter magnitude bins. The proper motion errors scale inversely with epoch difference. The greater depth of the Bok survey is evident, obtaining comparable proper motion errors roughly 0.75 mag fainter than the 1.3m survey. At their 95% completeness limits ($r = 22.0$ for the Bok survey, and $r = 20.9$ for 1.3m survey), both surveys have mean proper motion errors of about 15 mas year^{-1} (for an epoch difference of six years).

The mean proper motion for all QSOs in the Bok survey is 0.5 mas year^{-1} in right ascension and 0.3 mas year^{-1} in declination, and for the 1.3m survey 0.7 mas year^{-1} in right ascension and 0.1 mas year^{-1} in declination. The expected error in the mean is about 0.05 mas year^{-1}, thus the mean motions represent real systematic errors. There is no magnitude dependence for the mean motions. 0.6% of the Bok QSOs, and 0.4% of the 1.3m QSOs, have proper motions greater than three times their proper motion errors, compared with the 0.3% expected for a normal distribution. Figures 11 and 12 show the distribution of mean proper motions across the focal plane (the expected error in the mean for each bin is around 0.5 mas year^{-1}). There are no evident systematics across either focal plane. Figure 13 displays the distribution of mean proper motions across the northern galactic cap region of the survey, binned in 100 square degree segments of sky. Each bin contains more than 300 stars, yielding an expected error in the mean motions of less than 0.3 mas year^{-1}. There are some large scale systematic mean motions, particularly in declination, of up to 1 mas year^{-1}. DCR effects are one possible source of such systematics, as QSOs have very different spectral energy distributions from stars, and the fields at low and high right ascension within the north galactic cap region tend to be observed further from the meridian and at higher zenith distance. The SDSS+USNO-B survey shows similar systematics (Bond et al. 2010), and these will propagate to our survey since the SDSS+USNO-B proper motions are used to propagate the SDSS positions to the survey epoch.

The most complete, deep, wide-area proper motion catalog available for comparison is the LSPM catalog (Lépine & Shara 2005; we don't use the SDSS+USNO-B catalog for this purpose, since it provides our astrometric calibrators, nor the USNO-B catalog, since it has a large contamination rate at large proper motions). The catalog is based on the Space Telescope Science Institute scans of the POSS-I and POSS-II Schmidt plates. It improves on other high-proper-motion catalogs based on the POSS plates in using an image subtraction technique, which allows them to achieve an estimated completeness of 99% at high Galactic latitudes for $V < 19$ and proper motions larger than 0.15″ year^{-1} (the current published catalog is for stars north of the celestial equator). We can thus measure our completeness by comparison with LSPM stars in the magnitude range $16 < V < 19$, where the bright limit avoids saturated stars in our survey, and the faint limit corresponds to the faint limit of the LSPM survey. There are 5410 LSPM stars in that magnitude range in our survey footprint, of which all but 114 have a matching catalog entry in our survey, for a completeness rate of 97.9%. The completeness is a function of total proper motion, falling from 99% for a total proper motion of 150 mas year^{-1} to 94% for a total proper motion of 700 mas year^{-1}. Three of the unmatched LSPM stars are false detections in LSPM, which becomes apparent with the two additional CCD epochs. Another 99 of the unmatched LSPM stars are close pairs of detections in the SDSS survey but single (unresolved) detections in our survey, in which the LSPM star is matched to one detection in the SDSS pair, and our detection is matched to the other SDSS detection. Of these 99 cases, 51 are clearly pairs of blended stars which are resolved as two stars in the SDSS catalog, but unresolved in our survey, while the remaining appear by eye to be multiple detections of the same single star in the SDSS image, though it's certainly possible that they are indeed blended pairs of stars resolved by the SDSS object detection algorithm but too close to be obviously two stars by eye inspec-

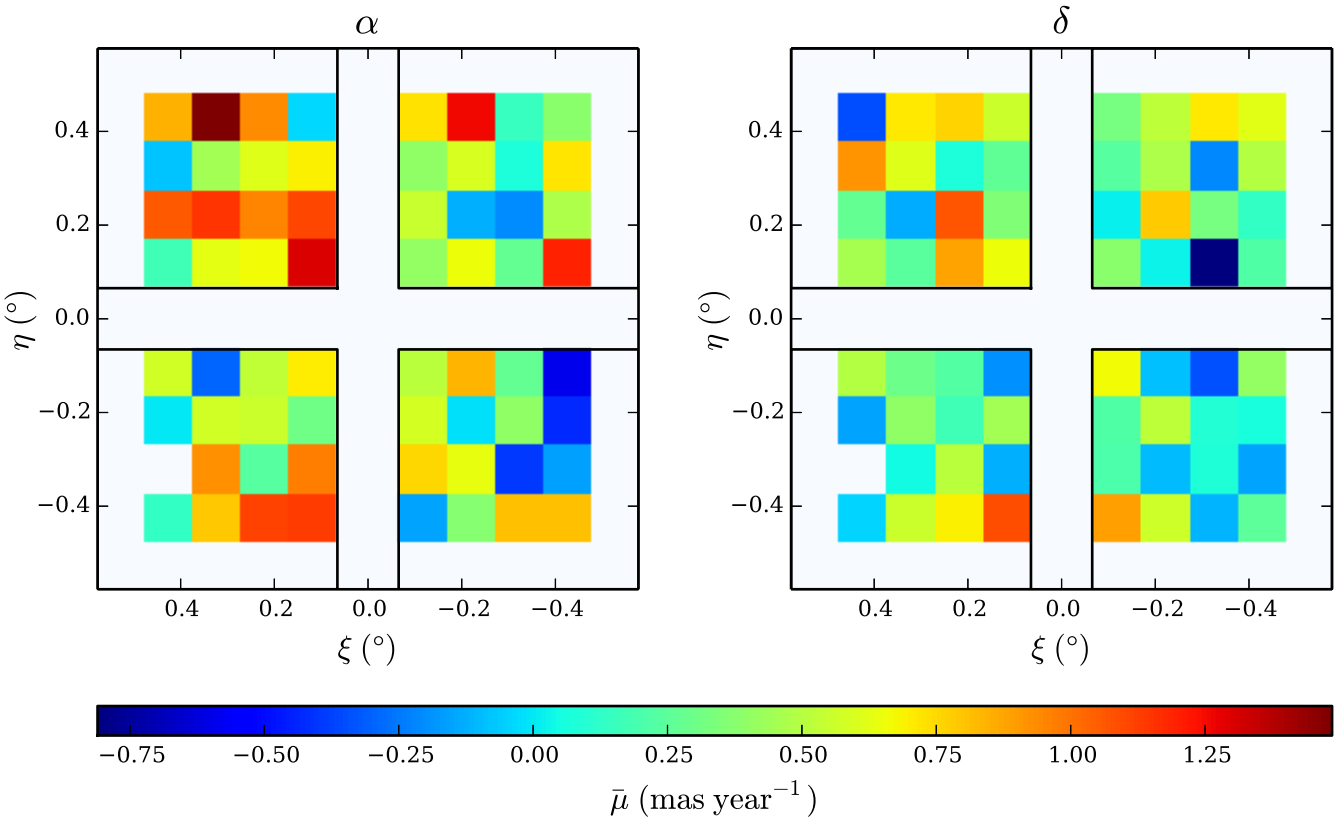

Figure 11. Mean proper motion of QSOs binned across the Bok focal plane. Proper motions in right ascension are shown in the left figure, and in declination in the right figure. The white bins along the edges of the focal plane have too few QSOs for a proper measure, due to overlap between fields.

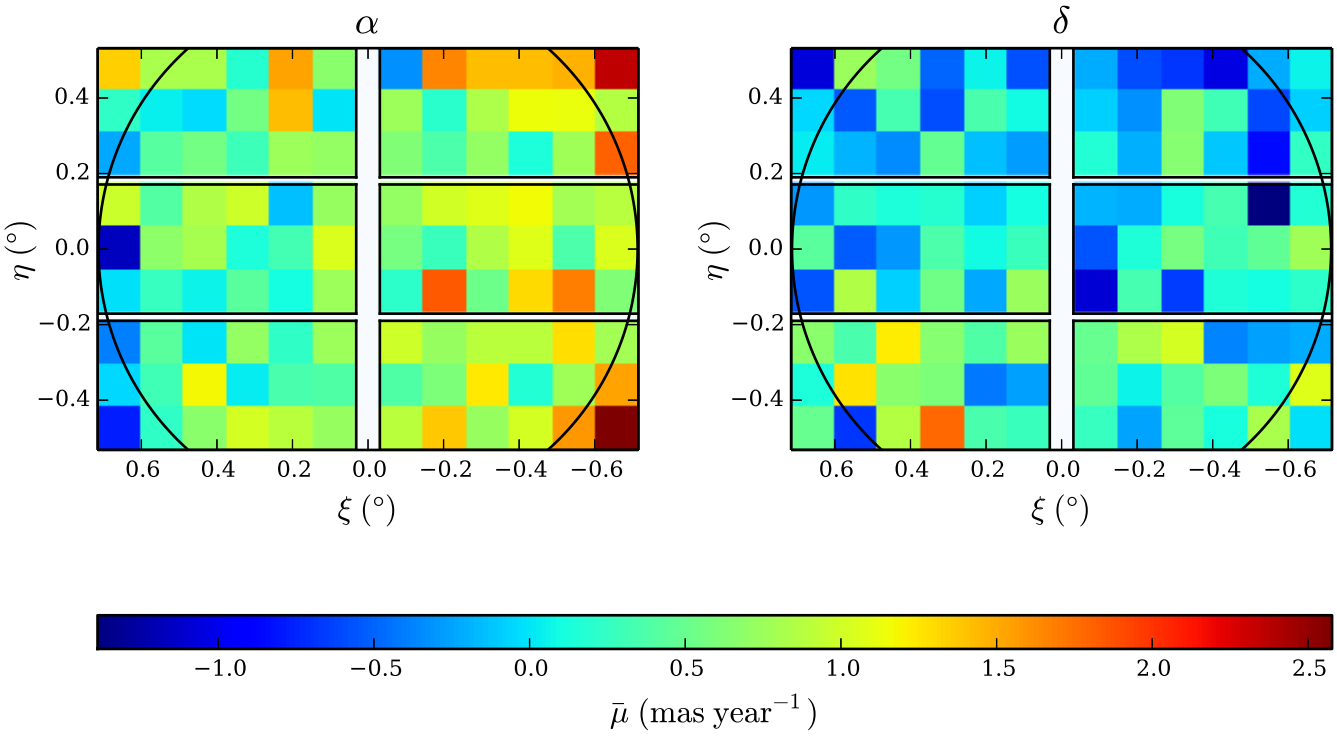

Figure 12. Mean proper motion of QSOs binned across the 1.3m focal plane. Proper motions in right ascension are shown in the left figure, and in declination in the right figure. A circle with radius 0.7 degrees is shown for reference.

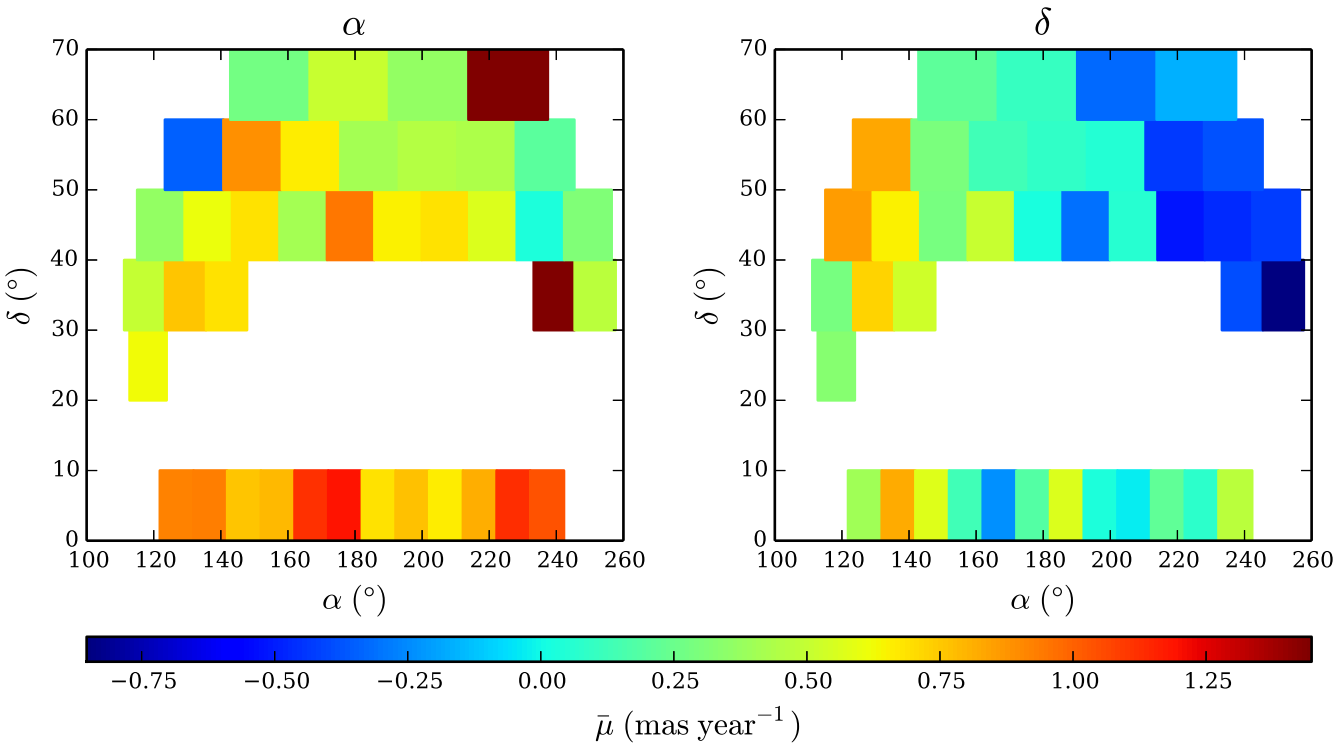

Figure 13. Mean proper motion of QSOs in 100 square degree bins in the north galactic cap region of the survey. Proper motions in right ascension are shown in the left figure, and in declination in the right figure.

tion. One LSPM star falls in an apparent hole in the SDSS data which is not listed in the DR7 hole list. The remaining 11 unmatched LSPM stars are located near very bright stars, and undetected in our survey either because they were lost in the scattered light of the bright star, or were blended with a diffraction spike from the star.

For the LSPM stars that have matching entries in our catalog, 188 have proper motions in our catalog which disagree with the LSPM proper motions by more than three times the expected errors. Of these, 24 are false detections in the LSPM catalog, which again is apparent with the additional CCD epochs. For an additional 77, our proper motions are clearly better than the LSPM proper motions, due primarily to better resolution of blended stars or deeper exposures of faint stars on the CCD images versus the Schmidt plates. Thus, only 87 of our proper motions are suspect, for a contamination rate of 1.6%. This rate may be an overestimate, as for 20 of the 87, it is not clear by eye inspections of the images that either our or the LSPM proper motions are wrong. The remaining 67 objects clearly have errant proper motions in our catalog. Of these, three have problems with the SDSS detection, while the remaining 64 are errant detections in our survey, due primarily to blends with other stars or diffraction spikes, mismatches, or poor centers.

There are 214 pairs of observations where the same target field was observed with both the Bok and 1.3m telescopes, and each observation in the pair was of "good" quality. These cover 130 square degrees of the survey, providing repeat observations of 536,630 SDSS stars in the magnitude range $16 < r < 21.5$, which can be further used to examine the survey completeness and contamination. A total of 98.4% of the stars were detected in the Bok observations, 97.5% were detected in the 1.3m observations, and 96.8% were detected in both the Bok and 1.3m surveys. For those stars detected in both surveys, 98.5% have proper motions which agree within three times the expected errors. Assuming these proper motions are thus correct (in some cases we can certainly have matching yet incorrect proper motions, such as the same mismatch in both surveys, however based on the comparisons with LSPM discussed above these should be rare), this yields a contamination rate of 1.5%, in good agreement with the contamination rate based on the LSPM analysis. Figure 14 displays histograms of the mean differences between the Bok and 1.3m proper motions in individual fields. Systematic differences are consistently less than 0.5 mas year^{-1}.

For a survey as large as this, even a 1.5% contamination rate yields a large number of objects with incorrect proper motions, and the contamination rate is expected to increase with increasing proper motion. The primary science driver for the catalog is to generate a large statistically well-defined sample of faint proper motions for Galactic structure studies. We are more interested in pushing the catalog to small proper motions, so as to increase the sample size and depth, than we are in generating a complete and contamination free sample of high proper motion stars. The latter is beyond the scope of the paper. However we can use both the LSPM matches and duplicate detections to help isolate sets of cuts to the catalog so as to remove some fraction of contaminants while maintaining a high completion rate. Table 1

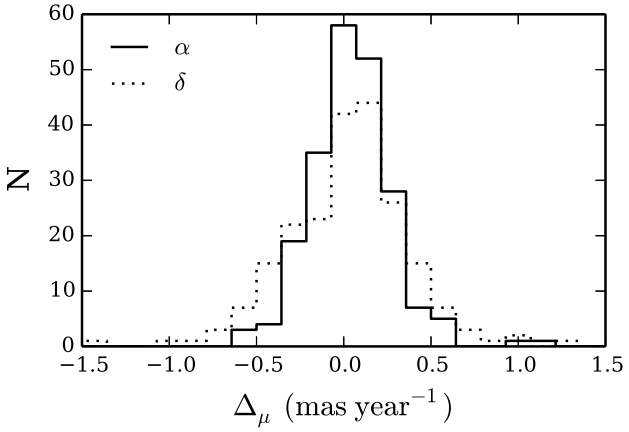

Figure 14. Distribution of mean differences between Bok and 1.3m proper motions in individual duplicate fields. Solid and dotted histograms are the distributions for proper motions in right ascension and declination, respectively.

presents such a set of cuts. For each cut, we list the fraction of our stars that we consider as good or bad detections, based on matches with the LSPM catalog, which meet the cut. Similar results are listed based on our analysis of duplicate detections between the Bok and 1.3m surveys. An ideal cut would retain most of the good objects, while rejecting a large fraction of the bad objects. While all of the proposed cuts retain at least 97% of the good objects, none reject more than half of the bad objects. The PSF fitting is adversely affected by the fixed pattern noise on CCD 2 in the Bok survey. In cases where statistics vary significantly between the Bok CCD 2 data and the rest of the survey, the statistics for the Bok CCD 2 data are given in the footnotes, and the data for the rest of the survey are given in the table. It is also the case that the worst of the FOV-dependent systematic errors in the proper motions for the Bok survey occur on CCD 2. Those applications which require the smallest systematics may wish to exclude the data from CCD 2 for the Bok survey.

4.3. *Photometry*

We examine the accuracy of the photometry error estimates by examining the distribution of magnitude differences between the SDSS magnitudes and our magnitudes, divided by the estimated errors in the differences. If our (and SDSS's) error estimates are accurate, the distributions should be Gaussian with standard deviations of one. Figure 15 displays histograms of the standard deviations of normalized errors for each image of quality "good", for stars in the magnitude range $17 < r < 21.5$. Typically, the Bok errors are underestimated by about 10%, and the 1.3m errors by about 15%. The Bok distribution shows a tail of images whose errors are overestimated by 10 – 40%; these are all from CCD 2, and are an effect of the fixed pattern noise on that CCD. Figure 16 displays the mean standard deviation in half magnitude bins, separately for each survey. Both surveys overestimate the errors at the bright end by about 20%, indicating likely overestimated calibration errors, while underestimating at the faint end by about 20%.

The dependence of photometric errors on magnitude is shown in Figure 17. The mean photometric errors for a

Table 1
Catalog Cuts

Cut	LSPM Good (%)	LSPM Bad (%)	Duplicates Good (%)	Duplicates Bad (%)
Good SDSS detection[a]	100.0	91.9	100.0	100.0
SExtractor detection[b]	98.4	66.6	98.4	76.8
1-to-1 match[c]	98.3	87.7	100.0	83.8
nIter < 10[d]	98.9[e]	59.5	99.1	53.1
chi < 8[f]	97.6[g]	57.8	99.2[h]	71.3
$\|\dot{\Delta}_r\| < 0.5$[i]	99.4[j]	61.6	99.4	59.4

[a] A clean SDSS detection, requiring the SDSS flag combination BINNED1 & !(BRIGHT | NOPROFILE | DEBLEND_NOPEAK).
[b] Detected using SExtractor.
[c] Exactly one object in this survey matched exactly one SDSS object.
[d] The number of iterations when fitting this object to the PSF in DAOPHOT. 10 was the maximum number of iterations allowed, thus objects with nIter = 10 were not well fit by the PSF.
[e] Excludes Bok CCD 2; 96.1% for Bok CCD 2.
[f] DAOPHOT chi parameter.
[g] Excludes Bok CCD 2; 62.8% for Bok CCD 2.
[h] Excludes Bok CCD 2; 89.2% for Bok CCD 2.
[i] Absolute difference between the SDSS r magnitude and our magnitude.
[j] Excludes Bok CCD 2; 96.5% for Bok CCD 2.

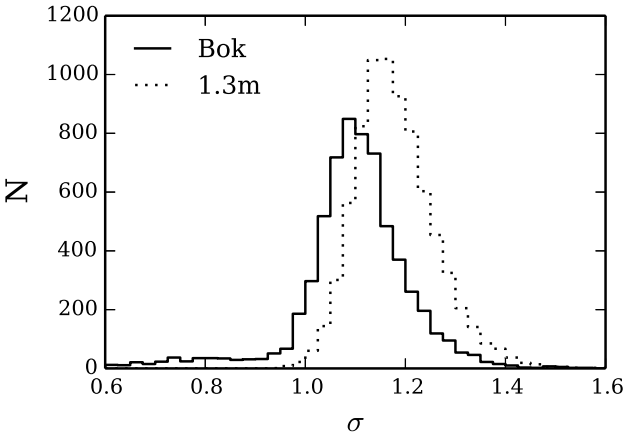

Figure 15. Distribution of the standard deviation in each field of the difference between SDSS and our magnitudes, normalized by the expected errors in the differences, for "good" fields only. Solid and dotted histograms are for the Bok and 1.3m surveys, respectively. Perfectly estimated errors would yield a standard deviation of one.

sample of clean stars in fields of quality "good" are plotted in quarter magnitude bins. At their 95% completeness limits ($r = 22.0$ for the Bok survey, and $r = 20.9$ for 1.3m survey), both surveys have mean photometric errors of about 0.07 magnitudes.

5. THE CATALOG

The observations reported here add proper motions and a second epoch of r band photometry to a portion of the SDSS DR7 catalog. Any science conducted with the catalog will rely on SDSS DR7 for its precise 5-band photometry, morphological classification, extinction estimates, etc. Rather than duplicate the SDSS DR7 data, we make our catalog available within the SDSS Catalog

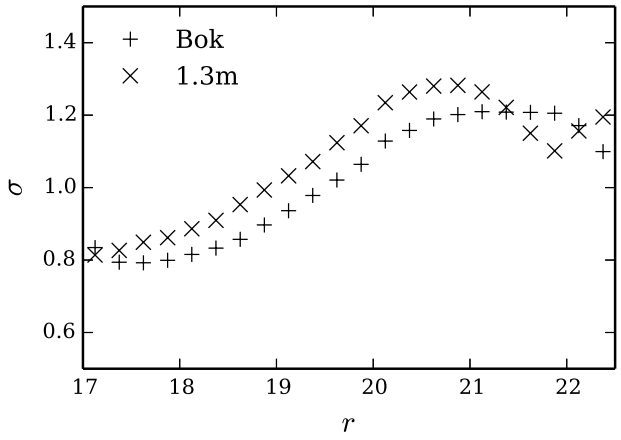

Figure 16. Mean standard deviation of the difference between SDSS and our magnitudes, normalized by the expected errors in the differences, for "good" fields only, versus r magnitude. Pluses and crosses are the standard deviations for the Bok and 1.3m surveys, respectively. Perfectly estimated errors would yield a standard deviation of one.

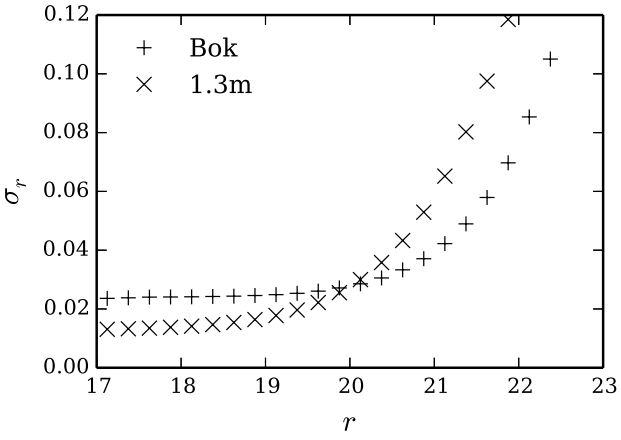

Figure 17. Mean photometric error as a function of r magnitude, for a sample of clean stars with a field quality of "good". Pluses and crosses are for the Bok and 1.3m surveys, respectively.

Archive Server Jobs System (CasJobs)[3]. The data are contained in four tables in the special user "deepPM"'s MyDB that are published to the "public" group so that they are available to all users of the CasJobs system. These tables have links to the matching SDSS objects in the DR7 context (see sample query below for the syntax to reference these tables and link them to the DR7 data).

The first table, "Observation", has an entry for each observation in the survey (excluding "bad" observations). The schema is given in Table 2. The area of sky covered by each image is the intersection of the CCD footprint and SDSS areal coverage, excluding bad regions of the CCD. We have used MANGLE[4] (Hamilton & Tegmark 2004; Swanson et al. 2008) to define the sky coverage for each image. Further, we have adopted the bright star masks of Blanton et al. (2005, reproducing the algorithm for some of the southern SDSS stripes not included in that paper) to optionally exclude

[3] http://skyserver.sdss.org/casjobs/
[4] http://space.mit.edu/∼molly/mangle/

regions affected by bright stars. In the "Observation" table, the attributes "fullAreaX" give the full areal coverage for CCD X, while "areaX" gives the areal coverage exluding the bright star masks. The spherical polygons comprising the MANGLE descriptions of the sky coverage for each image are given in the table "Cap", whose schema is given in Table 3. The nomenclature follows that of MANGLE's "polygon" file format. Each image (identified by the combination of columns "night", "obsID", and "ccd") is covered by the union of one or more polygons, and each polygon is defined by the intersection of spherical caps. Two separate sets of polygons are given for each image, one which excludes regions affected by bright stars, and one which does not.

Each SDSS DR7 star or galaxy that falls within our survey area, and within a given r magnitude range, is listed in the tables "PMStar" or "PMGalaxy", respectively. For the Bok survey, we include SDSS objects in the magnitude range $16 \leq r \leq 23$, while for the 1.3m survey we include objects in the magnitude range $15 \leq r \leq 22$ (using PSF magnitudes for stars and model magnitudes for galaxies). The bright limits are determined by the onset of saturation for stars, and the faint limits are set to one magnitude below the approximate 95% completeness limits. There is a table entry for each SDSS object, whether or not it was detected in our survey. Unmatched SDSS objects will have the column "match" set to 0. Objects in our survey are matched to SDSS objects by searching in annuli using progressively larger radii. If more than one match is found within an annulus, the nearest match is used. While galaxies will not have detectable proper motions in our survey, we list proper motions for galaxies because the SDSS star/galaxy classification is not perfect, particularly at the faint end of our survey, and some users may choose to use their own morphological classifications. The measured proper motions of galaxies also provide additional quality analysis, in the same way the measured proper motions of QSOs do. The schema for the "PMStar" and "PMGalaxy" tables is given in Table 4. In addition to links to the matching SDSS objects, and to the observations in our survey in which the SDSS objects should have been detected, the tables list the proper motions in right ascension and declination, their uncertainties, the r magnitudes in our survey (derived from the PSF fits, even for galaxies) and their uncertainties, various parameters characterizing the PSF fits as produced by DAOPHOT, and various image parameters produced by SExtractor. Some matched objects lack either DAOPHOT or SExtractor (but not both) measurements, in which case those attributes will be set to 0. Only objects successfully measured by DAOPHOT have measured proper motions, since the proper motions are based on the DAOPHOT centers. The "PMStar" table contains 21,157,643 entries, of which 18,982,227 have measured proper motions in our survey, and the "PMGalaxy" table contains 33,782,162 entries, of which 25,506,247 have measured proper motions in our survey.

The tables are public tables in the SDSS CasJobs. Refer to the CasJobs documentation for instructions on accessing public tables. As an an example of accessing the data, executing the following batch SQL query within the DR7 context in CasJobs will return SDSS positions and *ugriz* photometry, along with our proper motions, for all stars in the Bok survey that: (1) have a "good" observation in our survey, (2) have a one-to-one match between SDSS and our survey, (3) are in the magnitude range $20 < r < 22$, and (4) have a proper motion greater than 100 mas year^{-1}:

```
SELECT s.ra, s.dec, s.psfMag_u, s.psfMag_g,
       s.psfMag_r, s.psfMag_i, s.psfMag_z,
       p.pmRa, p.pmDec
FROM public.deepPM.PMStar p
JOIN public.deepPM.Observation o ON
     p.night = o.night AND p.obsID = o.obsID
JOIN Star s ON p.objID = s.objID
WHERE o.survey = 0 AND
      o.quality = 1 AND
      p.match = 11 AND
      s.psfMag_r BETWEEN 20 and 22 AND
      p.pmRa * p.pmRa + p.pmDec * p.pmDec >
      100 * 100
```

6. SUMMARY

We have obtained second epoch imaging over 3100 square degrees of sky within the SDSS footprint, and combined these data with SDSS astrometry to generate a deep proper motion catalog. The catalog includes:

- 1098 square degrees of sky, 95% complete to $r = 22.0$, based on observations in good observing conditions with the 90prime camera on the Steward Observatory Bok 90 inch telescope;
- 1521 square degrees of sky, 95% complete to $r = 20.9$, based on observations in good observing conditions with the Array Camera on the USNO, Flagstaff Station, 1.3 meter telescope;
- and an additional 488 square degrees of sky of lesser quality data, obtained under poor seeing or partially cloudy skies on both telescopes.

The catalog provides both absolute proper motions (on the system of the SDSS+USNO-B catalog) and a second epoch of r band photometry. The statistical errors for the proper motions range from roughly 5 mas year^{-1} at the bright end, to 15 mas year^{-1} at the survey completeness limits, for a typical epoch difference of 6 years. The systematic errors for the 1.3m are less than 1 mas year^{-1}. For the Bok survey, there are FOV-dependent systematic errors of as high as 2 – 4 mas year^{-1}, though typically less than that. The statistical errors for the r photometry varies from 0.01 – 0.02 magnitudes at the bright end to about 0.07 magnitudes at the completeness limits.

Comparison with the LSPM high proper motion catalog, as well as using duplicate observations between the Bok and 1.3m surveys, indicates a completeness rate of 98% (falling from 99% at a total proper motion of 150 mas year^{-1} to 94% at a total proper motion of 700 mas year^{-1}), and a contamination rate of false proper motions of 1.5%. The catalog is available in the SDSS CasJobs.

We thank Ani Thakar for support loading the catalog into the SDSS CasJobs. We also thank Mike Lesser,

Table 2
Observation Schema

Name	Type	Units	Description
night[a]	int32		MJD number of the night the observation was obtained.
obsID[a]	int16		Observation number, unique within a given night.
survey	int8		Which survey is this observation part of: 0=Bok, 1=1.3m.
mjd	float64		MJD at start of the observation.
expTime	float32	seconds	Exposure time.
ra	float64	degrees	Right ascension of target field center.
dec	float64	degrees	Declination of target field center.
fwhm	float32	arcsecs	Average FWHM over all CCDs.
sky	float32	mags arcsec^{-2}	Average sky brightness over all CCDs.
zero	float32	mags	Average photometric zeropoint over all CCDs.
raRms	float32	arcsecs	Average astrometric calibration rms residual in right ascension over all CCDs.
decRms	float32	arcsecs	Average astrometric calibration rms residual in declination over all CCDs.
quality	int8		Data quality: 1=good, 0=ok.
ccd1	int8		Is data for CCD 1 included in the survey: 1=yes, 0=no.
fullArea1	float32	degrees^2	Area of sky covered by CCD 1, including regions affected by bright stars.
area1	float32	degrees^2	Area of sky covered by CCD 1, excluding regions affected by bright stars.
minDT1	float32	years	Minimum epoch difference for all objects on CCD 1.
fwhm1	float32	arcsecs	FWHM on CCD 1.
sky1	float32	mags arcsec^{-2}	Sky brightness on CCD 1.
zero1	float32	mags	Photometric zeropoint on CCD 1.
raRms1	float32	arcsecs	Astrometric calibration rms residual in right ascension on CCD 1.
decRms1	float32	arcsecs	Astrometric calibration rms residual in declination on CCD 1.
psfRms1	float32	mags	Photometric calibration rms residual on CCD 1.
ccd2	int8		Is data for CCD 2 included in the survey: 1=yes, 0=no.
fullArea2	float32	degrees^2	Area of sky covered by CCD 2, including regions affected by bright stars.
area2	float32	degrees^2	Area of sky covered by CCD 2, excluding regions affected by bright stars.
minDT2	float32	years	Minimum epoch difference for all objects on CCD 2.
fwhm2	float32	arcsecs	FWHM on CCD 2.
sky2	float32	mags arcsec^{-2}	Sky brightness on CCD 2.
zero2	float32	mags	Photometric zeropoint on CCD 2.
raRms2	float32	arcsecs	Astrometric calibration rms residual in right ascension on CCD 2.
decRms2	float32	arcsecs	Astrometric calibration rms residual in declination on CCD 2.
psfRms2	float32	mags	Photometric calibration rms residual on CCD 2.
...[b]			

[a] The combination of columns "night" and "obsID" uniquely identify an observation, and together comprise the primary key for the table.
[b] The attributes "ccdX" – "psfRmsX" are repeated for CCDs (X) 3 – 6. For the Bok survey, the attributes for CCD 5 and 6 will all be set to 0, since the camera only has 4 CCDs.

Table 3
Cap Schema

Name	Type	Units	Description
night	int32		MJD number of the night the observation was obtained.
obsID	int16		Observation number.
ccd	int8		CCD covered by this cap.
brightStar	int8		1=excludes regions affected by bright star masks, 0=doesn't.
polygon	int8		Identifier of polygon to which this cap belongs.
x	float64		X component of the unit vector defining the north polar axis of the cap.
y	float64		Y component of the unit vector defining the north polar axis of the cap.
z	float64		Z component of the unit vector defining the north polar axis of the cap.
cm	float64		1 - cos(θ), where θ is the polar angle of the cap. Positive/negative cm designates the region north/south of the polar angle.

Edward Olszewski, and Grant Williams for their outstanding work building 90Prime, and Fred Harris for his outstanding work building the Array Camera. MK gratefully acknowledges the support of the NSF under grant AST-1312678 and NASA under grant NNX14AF65G. KW gratefully acknowledges the support of the NSF under grants AST-0206084 and AST-0602288. This material is also based on work supported by the National Science Foundation under grant AST 06-07480.

Funding for the SDSS and SDSS-II has been provided by the Alfred P. Sloan Foundation, the Participating Institutions, the National Science Foundation, the U.S. Department of Energy, the National Aeronautics and Space Administration, the Japanese Monbukagakusho, the Max Planck Society, and the Higher Education Funding Council for England. The SDSS Web Site is http://www.sdss.org/. The SDSS is managed by the Astrophysical Research Consortium for the Participating Institutions. The Participating Institutions are the American Museum of Natural History, Astrophysical Institute Potsdam, University of Basel, University of Cambridge, Case Western Reserve University, University of Chicago, Drexel University, Fermilab, the Institute for Advanced Study, the Japan Participation Group, Johns

Table 4
PMStar/PMGalaxy Schema

Name	Type	Units	Description
objID	int64		Unique SDSS identifier for the SDSS object.
night	int32		MJD number of the night the observation was obtained.
obsID	int16		Observation number.
ccd	int8		CCD on which the object was or should have been detected.
brightStar	int8		1 if objects falls in a masked region around a bright star, else 0.
match	int16		Multiplicity of matches between our survey and SDSS. Ones digit indicates number of matching objects in SDSS, and 10s digit indicates number of matching objects in this survey. Thus, 11 indicates a one-to-one match. If 0, there was no match for this SDSS object in our survey, and all remaining columns for this object will be set to 0.
pmRa	float32	mas year^{-1}	Proper motion in right ascension, along the great circle (i.e., $\dot{\alpha}\cos(\delta)$).
pmRaErr	float32	mas year^{-1}	Error in proper motion in right ascension.
pmDec	float32	mas year^{-1}	Proper motion in declination.
pmDecErr	float32	mas year^{-1}	Error in proper motion in declination.
r	float32	mags	r magnitude in our survey.
rErr	float32	mags	Error in r magnitude.
x	float32	pixels	X-axis coordinate of object center.
y	float32	pixels	Y-axis coordinate of object center.
nIter	int8		Number of iterations when DAOPHOT fit the PSF. The maximum is 10 iterations, thus a value of 10 indicates possible problems fitting the PSF. A value of zero indicates the object was not successfully measured by DAOPHOT, thus there is no photometry nor measured proper motions for this object (columns pmRa, pmRaErr, pmDec, pmDecErr, r, rErr, chi, sharp, and skyMode will all be 0).
chi	float32		DAOPHOT estimate of the ratio of the observed pixel-to-pixel scatter from the model image divided by the expected pixel-to-pixel scatter from the image profile.
sharp	float32		DAOPHOT sharpness.
skyMode	float32	mags arcsec^{-2}	DAOPHOT mode of the local sky histogram.
flags[a]	int32		SExtractor flags. See SExtractor documentation for description of bit values.
awin_image	float32	pixels	SExtractor windowed semi-major axis length.
errawin_image	float32	pixels	Error in SExtractor windowed semi-major axis length.
bwin_image	float32	pixels	SExtractor windowed semi-minor axis length.
errbwin_image	float32	pixels	Error in SExtractor windowed semi-minor axis length.
thetawin_image	float32	degrees	SExtractor position angle of the semi-major axis.

[a] The saturation level was incorrectly set for the Bok data, and thus the saturation bit for that data should be ignored.

Hopkins University, the Joint Institute for Nuclear Astrophysics, the Kavli Institute for Particle Astrophysics and Cosmology, the Korean Scientist Group, the Chinese Academy of Sciences (LAMOST), Los Alamos National Laboratory, the Max-Planck-Institute for Astronomy (MPIA), the Max-Planck-Institute for Astrophysics (MPA), New Mexico State University, Ohio State University, University of Pittsburgh, University of Portsmouth, Princeton University, the United States Naval Observatory, and the University of Washington.

Facilities: Bok (90prime), USNO:1.3m (Array Camera)

REFERENCES

Abazajian, K. N., Adelman-McCarthy, J. K., Agüeros, M. A., et al. 2009, ApJS, 182, 543
Aihara, H., Allende Prieto, C., An, D., et al. 2011, ApJS, 193, 29
Ahn, C. P., Alexandroff, R., Allende Prieto, C., et al. 2012, ApJS, 203, 21
Bertin, E. & Arnouts, S. 1996, A&AS, 117, 393
Blanton, M. R., Schlegel, D. J., Strauss, M. A., et al. 2005, AJ, 129, 2562
Bond, N. A., Ivezić, Ž., Sesar, B., et al. 2010, ApJ, 716, 1
Fukugita, M., Ichikawa, T., Gunn, J. E., et al. 1996, AJ, 111, 1748
Gould, A. & Kollmeier, J. A. 2004, ApJS, 152, 103
Gunn, J. E., Carr, M., Rockosi, C., et al. 1998, AJ, 116, 3040
Gunn, J. E., Siegmund, W. A., Mannery, E. J., et al. 2006, AJ, 131, 2332
Hamilton, A. J. S. & Tegmark, M. 2004, MNRAS, 349, 115
Harris, H. C., Munn, J. A., Kilic, M., et al. 2006, AJ, 131, 571
Kilic, M., Munn, J. A., Harris, H. C., et al. 2006, AJ, 131, 582
Kilic, M., Munn, J. A., Williams, K. A., et al. 2010, ApJLett, 715, L21
Lépine, S. & Shara, M. M. 2005, AJ, 129, 1483
Munn, J. A., Monet, D. G., Levine, S. E., et al. 2004, AJ, 127, 3034
Munn, J. A., Monet, D. G., Levine, S. E., et al. 2008, AJ, 136, 895
Monet, D. G., Levine, S. E., Canzian, B., et al. 2003, AJ, 125, 984
Schneider, D. P., Richards, G. T., Hall, P. B., et al. 2010, AJ, 139, 2360
Stetson, P. B. 1987, PASP, 99, 191
Swanson, M. E. C., Tegmark, M., Hamilton, A. J. S., & Hill, J. C. 2008, MNRAS, 387, 1391
Tody, D. 1986, Proc. SPIE, 627, 733
Tody, D. 1993, in ASP Conf. Ser. 52, Astronomical Data Analysis Software and Systems II, ed. R.J. Hanisch, R.J.V. Brissenden, & J. Barnes (San Francisco, CA: ASP), 173
Williams, G. G., Olszewski, E., Lesser, M. P., & Burge, J. H. 2004, Proc. SPIE, 5492, 787
York, D. G., Adelman, J., Anderson, Jr., J. E., et al. 2000, AJ, 120, 1579